Combustion of coal mine ventilation air methane in a regenerative combustor with integrated adsorption: reactor design and optimization

Javier Fernández, Pablo Marín, Fernando V. Díez, Salvador Ordóñez*

Department of Chemical and Environmental Engineering, University of Oviedo, Facultad de Química, Julián Clavería 8, Oviedo 33006, SPAIN
* Phone: 34-985 103 437, FAX: 34-985 103 434, e-mail: sordonez@uniovi.es

Abstract

Coal mine ventilation air methane is an important environmental concern due to its contribution to global warming. Catalytic combustion in reverse flow reactors is an efficient treatment technique, but high emission moistures lead to catalyst inhibition. To overcome this issue a novel reverse flow reactor with integrated water adsorption has been proposed.

In this work, the design of a reverse flow reactor adequate to treat a typical real coal ventilation stream, 45 m^3/s with 0.30% (mol) methane and 5% (mol) water, has been studied. The performance of the reactor design has been simulated using a 1D heterogeneous dynamic model, previously validated with experimental results. Particular attention has been paid to reactor stability when water and methane feed concentration change upon time. Real coal mine ventilation air data have been used to produce realistic simulations. The optimization of the operating conditions (surface velocity and switching time) has been carried out based on the total cost of the reactor (considering fixed capital and 10-year variable cost).

Keywords: regenerative catalytic oxidizer; hybrid reactor; methane combustion; water inhibition; reverse flow reactor; dynamic modelling.

1. Introduction

In the last decades, environmental issues related to global warming have gained importance. Methane is considered a major contributor to global warming (second in importance, after carbon dioxide), with global atmospheric concentrations raising from a pre-industrial value of about 0.7 up to 1.8 ppm in 2014 [1]. The main anthropogenic sources of methane are coal mines, landfills, natural gas distribution systems, sewage systems, etc. [2]. It is well known that the global warming potential of methane is 25 times greater than that of carbon dioxide, and for this reason the combustion of methane to carbon dioxide before releasing to the atmosphere is environmentally beneficial, as it reduces greatly the net warming potential of the emissions [3].

Coal mining has an important negative impact in relation to greenhouse emissions, because important amounts of methane (concentration 0.1 to 1%) are released to the atmosphere during coal extraction [4]. Thus, ventilation air methane represents the main contribution (approximately 78%) to the carbon footprint of the coal mining activity [5].

Catalytic combustion is a very interesting alternative for the treatment of these emissions [6], because of its low energy consumption (especially if compared with thermal oxidation) and the negligible formation of noxious by-products, such as thermal NOx [7]. An appropriate option for the treatment of coal mine ventilation air methane is the use of regenerative catalytic oxidation (RCO) in a reverse flow reactor [8].

Reverse flow reactors (RFR) consist of a catalytic fixed bed reactor in which the feed flow direction is periodically reversed [9]. By selecting the appropriate switching time (t_{sw}), defined as the time elapsed between two consecutive flow reversals, a great amount of the heat released in the reaction can be stored inside the reactor in consecutive cycles, and therefore autothermal operation (e.g. without the addition of external heat or fuel) can be possible even

for very low concentration of hydrocarbons (1500 ppm methane) [10]. For higher hydrocarbon concentration, the energy released by the reaction can be also recovered [11].

The RFR potential advantages are a consequence of its forced unsteady state operation [12]. However, this can also be a drawback from the stability point of view, i.e. maintaining ignited operation under disturbances in flow rate or concentration. For example, if the feed is too lean, there is a risk of extinction, because the amount of heat released by the reaction is very low; in these situations the RFR heat regeneration capacity is crucial to maintain autothermal operation [13]. Under rich feed conditions, the heat released and accumulated in the reactor can result in too high bed temperatures, with the risk of causing catalyst thermal deactivation [14]. This issue has limited the industrial use of this type of reactors, and encouraged research in the development of suitable control systems [15].

The performance of the catalyst can be affected by the presence of other compounds, different from methane, in the ventilation air [16]. Water is usually present in high amounts (nearly at the saturation point), and it is well-known that water has a negative effect on the activity of supported precious metal catalysts [17]. Palladium catalysts on various supports, the most active for methane oxidation, have been studied by different authors with a general agreement in the existence of a reversible inhibitory effect of water [18]. This inhibition reduces the relative stability of the reverse flow reactor, and to overcome this, the reactor must be oversized, with the corresponding increase in purchase and operation costs.

One solution to avoid the decrease in catalyst activity caused by water is the use of a reverse flow reactor with integrated adsorption. Such a device, proposed by Bos et al. [19], consists of a reverse flow reactor in which the inert beds are replaced, at least partially, by an appropriate adsorbent material [20]. Thus, the water of the feed is retained in these adsorbent beds before reaching the central catalytic bed [21]. The adsorbent is regenerated in situ, because of the parabolic temperature profile that develops in reverse flow reactors, with high temperature in

the middle and low temperature at the sides. The temperature profile is not static, but moves in the direction of the flow, and produces a displacement of heat from the centre to the sides of the reactor. Thus, while feed water is being adsorbed at low temperature in the first adsorbent bed (in the corresponding direction of the flow), the water adsorbed in the previous cycle desorbs at a higher temperature from the adsorbent bed placed in the opposite side of the reactor.

The working principle of the reverse flow reactor with integrated adsorption was experimentally demonstrated in a previous work for methane oxidation in a bench-scale device [22]. In the same work, a mathematical model to simulate the behaviour of this reactor was proposed. This model accurately predicted the experimental results.

The aim of the present work is to apply all this knowledge on reverse flow reactors with integrated adsorption to the design and optimization of commercial scale devices for the treatment of methane emissions from coal mines. The scope of the work is summarized as follows. Firstly, emissions of methane from different coal mines are analysed to determine representative average methane and water concentrations. Then, a reverse flow reactor with integrated adsorption is specifically designed to deal with this emission. The performance of the proposed design is tested by means of simulations for different feed water concentrations. Then, the capacity of the reactor to deal with disturbances in the feed (e.g. methane concentration) is also evaluated. Finally the influence of operational conditions on the total cost is studied and the cost is optimised.

2. Materials and methods

2.1. Reverse flow reactor model

A mathematical model for reverse flow reactors should predict the dynamic evolution of concentration and temperature profiles. Phenomenological models based on mass and energy conservation equations have been found to simulate RFRs with good results [23]. In the context of a previous work, a 1D heterogeneous model was proposed and validated for the case of a reverse flow reactor with integrated adsorption [22]. Table 1 shows the set of partial differential equations corresponding to this model. These equations were obtained from conservation equations (mass and energy) applied separately to the gas and solid phases. Gas and solid mass balances are valid for both compounds, methane and water.

The mass and energy balances to the gas phase (equations of c_i and T_G) accounts for the following terms (in the order of appearance in the equation): accumulation, convective flow, dispersion and mass or heat transfer from/to the solid phase. The gas phase non-catalytic combustion of methane is not included in the model, being negligible compared to catalytic combustion at the operating temperature of the reactor. The change in velocity due to density is accounted for by means of the continuity equation: $v = v_0\ \rho_{G0}/\rho_G$, where $\rho_G = pM/RT_G$. Ideal gas law behaviour has been assumed.

The mass and energy balances to the solid phase (equations of n_i and T_S) consider the accumulation in the solid, dispersion (only for the energy balance), mass or heat transfer from/to the gas phase and reaction terms.

The resolution of the partial differential equations of the model requires a given set of initial and boundary conditions, shown in Table 2. The switch of the feed flow direction is modelled by shifting the boundary conditions at both sides of the reactor. The model has been solved

using the 'method of lines' programmed as a MATLAB code. This method, proved to be accurate in previous works [24], consists of approximating the space derivatives in a mesh of 400 nodes by finite differences obtained from Taylor polynomials. This number of nodes was found enough to provide a grid-independent solution. The resulting set of ordinary differential equations (with only one independent variable: time) is solved using a specific MATLAB function for stiff problems ("*ode15s*" function).

The physical, chemical and transport properties appearing in the equations of Table 1 must be specified to solve the model. Table 3 shows the geometrical and physical properties of the catalytic and adsorbent beds [22], while Table 4 summarizes the expressions used to calculate the chemical and transport properties. The catalytic bed considered is formed by blocks of a commercial monolith of 390 cpsi (cells per square inch) and square channels of 10^{-3} m side. The channel walls are covered by a washcoating layer (volume fraction, f_w = 26%) of average thickness, L_w = 76×10^{-6} m. The washcoating is porous (internal porosity, ϵ_{int} = 0.16, and average pore size, d_{pore} = 12×10^{-9} m) and is impregnated with the palladium active phase. Intrinsic reaction rate of methane oxidation was measured in the laboratory in a previous work and fitted to a Langmuir-Hinshelwood model capable of predicting catalyst inhibition caused by water (Table 4) [25]. Mass transfer inside the washcoating layer is taken into account by means of the internal effectiveness factor (η) and Thiele modulus (ϕ), which is calculated from the above-mentioned textural properties of the washcoating. Gas to solid mass and heat transport and axial dispersion are estimated using correlations from the literature specific for monoliths at laminar conditions (Table 4) [26].

The adsorbent bed consists of a random particles, γ-alumina pellets of 4 mm diameter. The adequacy of this adsorbent material was assessed in a previous work [22]. Its adsorption capacity was experimentally measured and equilibrium data fitted to a Freundlich model (Table 4). This model is used to calculate the gas concentration of water in the solid-gas

interphase. Mass transfer, experimentally found to play an important role in the adsorption of water, was modelled using the linear driving force model. The global mass transfer coefficient (K_C), which accounts for mass transfer external and internal to the particles, was measured experimentally and correlated with temperature (Table 4). Gas to solid heat transport and axial dispersion are estimated using correlations from the literature, specific for packed beds (Table 4) [26].

The physical properties of the gas have been considered equivalent to those of air and calculated using temperature-dependent expressions from the literature [27].

3. Results and discussion

3.1. Coal mine ventilation air emissions

In subterranean coal mining, methane must be diluted in the working area down to safety constraints. This is accomplished by the use of large axial fans that flows fresh air through the shaft, diluting the methane released during the mining activities. The lower explosive limit of methane in air is 5%, but methane concentration is usually reduced below 1%. The exhaust of the fans can contain other compounds, such as carbon dioxide, and trace amounts of hydrogen sulphide or sulphur dioxide. The amount emitted depends on the coal rank and depth of seam. For example, high-rank coals, such as anthracite, produce the highest methane emissions [2].

The composition of the ventilation air of different coal mines from Asturias (northwest Spain) has been measured experimentally, and the results are summarized in Table 5. No sulphur compounds were found in the exhaust [5]. The time-averaged methane concentration was found to range from 0.18 to 0.40%, depending on the mine site [5]. Methane concentration is not constant with time, and varies according to other factors, with atmospheric pressure being

the most important. Variations in methane concentration are illustrated in Figure 2 for mine site 1 and a monitoring period of 70 days, shown as an example. Methane concentration varies mostly within the range 0.25 % to 0.50 %, with average methane concentration 0.39 % (mol).

Water concentration in the ventilation air was found to greatly depend of ambient conditions. For this reason, the range of variation for the different mine sites is reported in Table 5, instead of the time-averaged value. As a general trend for all mine sites, water concentration varies within the range 2 to 5 % (mol).

3.2. Design of a reverse flow reactor

A reverse flow reactor will be designed to treat the ventilation air of mine site 1 (Table 5), considered representative of the coal mines of the Asturian region (Spain). The design is based on a total gas flow of 45 m^3/s at 1 atm and 25°C, with a nominal methane concentration of 0.30% (mol). As shown in Figure 2, this nominal concentration value is close to the lower concentration limit (0.25%) reported for this mine site. For the so called "base design" of the reactor, the feed will be considered to be free of water, and the reactor designed consists of a central catalytic bed and two heat-regeneration beds. A sketch of the reactor is shown in Figure 1. The design of the reactor with integrated adsorption is addressed in Section 3.3.

The reverse flow reactor will be designed to maintain stable operation with high conversion (99.9%) for the nominal concentration of 0.30% (vol.) methane. However, methane concentration varies with time, so the dynamic response of the reactor to these variations will be also studied afterwards. The design of the reactor involves calculating the total reactor length and diameter, and the length of the different beds of the reactor.

The catalytic bed consists of palladium-based monolithic blocks with a cell density of 390 cpsi (cell per square inch). This type of bed has two important advantages for the present case: low pressure drop at high gas flow rates, and reduction of diffusional resistances for the catalytic reaction. The latter is particularly important for fast reactions and catalysts based on precious metals, as the present case, because the precious metal is deposited only in a thin porous washcoating layer, so the reactants diffusion path is lower when compared to particulate catalyst, and the active phase is more effectively used [26].

The heat-regeneration beds consist of γ-alumina pellets of 4×10^{-3} m (this material will act also as adsorbent in Section 3.3). Random particle beds have higher pressure drop than monolithic beds, but in our opinion the advantages when used in the reverse flow reactor with integrated adsorption are more important. Unlike the catalyst, there are not expensive active phase dispersed in the adsorbent particles, so when diffusional limitations are important, there is not expensive precious metal unused in the inside of the pellet. The adsorbent must present a high adsorption capacity to prevent premature saturation of the adsorbent bed, and this is obtained with random particle beds. Another important advantage of random particle beds is their higher thermal inertia, which results in more efficient heat storage between cycle, and hence reactor stability [28].

The geometrical and physical properties of catalytic and inert beds were measured experimentally or taken from the literature, as summarized in Table 3 and 4.

Switching time (t_{sw}) is an important variable that affects the behaviour of the reactor. This parameter can be adjusted during operation to control the reactor (e.g. to avoid extinction or overheating). For the design of the reactor (reactor dimensions), an appropriate nominal switching time value is selected. When selecting switching time it should be considered that lower switching time decrease the required reactor size, but on the other hand, the contribution of the wash-out effect increases, and the lifespan of the valves and the flexibility

of the control system decrease. In the present work, and according to our experience, a value of t_{sw}= 240 s is chosen, considered a good balance between these factors [29]. This value will be optimized in section 3.5 according to an economic optimization.

The procedure for the model-based design of reverse flow reactors has been discussed and validated elsewhere [30]. The steps of the procedure are summarised as follows. First, a superficial velocity value is selected; this is required because reactor length, diameter and superficial velocity are not independent (one must be set to calculate the others). The value of 1 m/s was found to be appropriate in a previous work [30], but its influence will be studied in detail in section 3.5, in the scope of an economic optimization. Second, the reactor cross section diameter (circular section) or side (square section) is calculated for the actual gas flow rate (45 m^3/s): in this case, 7.57 m and 6.71 m, respectively. Third, the reactor length required to achieve 99.9% conversion is determined using the reactor mathematical model (methodology section). This cannot be done directly because the reactor length is an implicit variable that must be supplied to solve the model. Hence, the reactor length is determined by trial and error, simulating the reactor up to the pseudo-steady state for different lengths, until the desired 99.9% conversion is achieved. At this stage, all the reactor bed is considered to be catalytic. Following this procedure, a reactor length of 1.52 m was determined.

Finally, the last design parameter of the reactor is the length of the catalytic bed (once determined, the length of the adsorbent beds can be easy calculated from the total bed length). In reverse flow reactors, all the catalyst at temperature below the ignition temperature of the hydrocarbon/air mixture should be replaced by cheaper inert material (in the present work by an adsorbent material) [10]. The ignition temperature of methane in our catalyst is around 350°C, so the boundaries of the catalytic bed are directly determined from the simulated temperature profile at the middle of a cycle. Hence, the required length for central catalytic bed is 0.49 m, corresponding to a fraction of catalytic bed of 32%; the length

of the adsorbent beds situated at both sides of the reactor is 0.52 m each. The reactor equipped with these inert beds has been simulated to check all the constraints used in the design are fulfilled. The results of the simulation are summarized in Figure 3.

The simulated temperature and methane concentration profiles of Figure 3 clearly show the displacement of heat and concentration fronts inside the reactor. The catalytic bed is maintained at high temperature during a cycle, which results in high methane conversion and prevents the extinction of the reactor. In the adsorbent beds, the difference between the temperature profile at the beginning and end of cycle is an indication of the amount of heat stored in the bed. As shown in Figure 3, this difference is large, which is due to the high energy efficiency of the designed reactor.

3.3. Design of the integrated adsorption

In the reactor designed in Section 3.2, the influence of the feed moisture on the combustion has not been taken into account, as water is supposed to be separated in the adsorbent beds before reaching the catalytic bed. The design of the integrated adsorption consists of calculating the minimum length of adsorbent required to accomplish this at the reverse flow reactor operating conditions (mainly temperature profile). This has been done by simulating the reverse flow reactor designed in the previous section, fed with a ventilation air containing the same methane 0.30% (mol), and in addition 5% (mol) water. This water concentration is the highest registered during the monitoring of the ventilation air.

The evolution of water concentration profiles in gas and solid at the pseudo-steady state are depicted in Figure 4. It can be observed that the adsorbent bed captures the water from the gas in a small part of the bed situated close to the reactor inlet. This part of the bed has the lower temperature, and hence the highest adsorption capacity. Regarding the water

concentration profiles in the solid, it should be noted that at the beginning of the cycle the bed contains some adsorbed water from previous cycles. Desorption takes place when the flow is reversed and the high temperature wave from the centre of the reactor moves to the adsorbent bed, but complete water desorption does not occur at these operating conditions. The effective capacity of the adsorbent is the difference between the solid concentration profiles at the end and beginning of cycle.

Figure 5 shows the evolution of water concentration in the gas effluent at pseudo-steady state conditions. At the beginning of a cycle, the concentration is the highest, because water is being desorbing from an adsorbent with high water concentration (from the previous cycle). The effluent concentration decreases upon time, and close to the end of the cycle a marked decreased is observed, indicating that the adsorbent bed is approaching depletion. Although water desorption has not been complete, the degree of regeneration of the adsorbent is high enough as to deplete water from the feed in the next cycle.

The performance of the integrated adsorption has also been evaluated for different water feed concentrations in the range 2-5% (mol). The gas and solid water concentration profiles of the inert beds at the end of a cycle are depicted in Figure 6. These are the profiles just before the flow is reversed, and hence correspond to the maximum displacement of water in the adsorbent bed. When water feed concentration increases from 2 to 5% (mol), the adsorption equilibrium concentration increases from 7.5 to 11.7 mol/kg, as shown in Figure 6b., and more water can be retained by the adsorbent. However, the higher water feed concentration produces a displacement of the concentration profiles, which is nearly proportional to the increase in feed concentration. The minimum lengths of adsorbent bed required to adsorb all the feed water are 0.060, 0.071, 0.081 and 0.097 m, respectively for 2, 3, 4 and 5% (mol), respectively. Figure 6 also shows the profiles in the second adsorbent bed (BED2), where in this cycle desorption is taking place. The solid profiles are particularly interesting, showing the

adsorbed water that does not desorb between cycles. The behaviour is inherent to every temperature-swing adsorption processes, and its consideration is very important in order to not underestimate the required amount of adsorbent.

It can be concluded that in the present reactor design and conditions, at least 0.1 m of adsorbent is required in each inert bed to separate the water from the ventilation air (2-5%). In the remaining inert bed (0.42 m each), the adsorbent can be replaced by a cheaper inert material with thermal properties more suited for regenerative devices. In this context, a material of high thermal inertia, $\rho_S(1-\epsilon_b)C_{PS}$, is advised (at least more than 700 kJ/m$^3_{bed}$ K).

3.4. Analysis of the reactor stability

The reactor stability can be affected by changes in feed conditions, such as gas flow rate and methane and water concentration, or operational parameters, like switching time. In the previous section, it was demonstrated that the integrated adsorption system is capable of separating water within the concentration range typically found in coal mine ventilation air flows. The air flow rate is directly related to the power and performance of the fan that propels the air, and the fan is usually operated at constant nominal conditions. For this reason, no important fluctuations in the flow rate are expected. Hence, this section is devoted to analyse the capacity of the designed reverse flow reactor to cope with disturbances in methane feed concentration, which have been observed experimentally in real emissions, and are directly related to the reactor thermal behaviour and stability.

First, the influence of a step decrease in methane concentration has been considered. Temperature and methane concentration profiles at the middle of cycle are depicted in Figure 7. Initially, the reactor was simulated up to the pseudo-steady state at 0.30% vol. methane (the concentration used in the reactor design). Then, concentration was decreased to 0.27% for 16

min (4 cycles). This disturbance produces a clear decrease in the reactor temperature, related to the lower amount of heat released by the reaction. However, this decrease in temperature is not critical, and the reactor remains stable with high methane conversion, as observed in the concentration profile. Finally, the concentration was increased back to 0.30% methane. The reactor temperature exhibits a sudden increase to the initial temperature profile. This indicates that, within a certain margin, changes in concentration do not produce a permanent effect in the performance of the reactor, and the reactor does not extinguish.

The reactor performance was studied simulating its response to a real evolution of methane concentration in a coal mine ventilation air was. Figure 8 shows the evolution of methane concentration in the ventilation air, with an average value of 0.30% (vol.) methane and positive and negative variations within the range ±0.05%. The corresponding reactor outlet methane concentration obtained by simulation is depicted in the same figure. It is clearly observed that the reactor is capable of operating at stable conditions with high conversion under these real feed disturbances. Temperature and methane concentration profiles are presented in Figure 9, where different situations, representative of high and low methane feed concentrations, are considered. Thus, it can be seen that the temperature profile moves in the vertical direction, with a maximum within the range 485-528°C. This temperature range is adequate, because it is below the catalyst overheating limit and above the reaction extinction limit.

It can be concluded that, in the conditions studied, representative of the treatment of real coal ventilation streams, the operation of the reverse flow reactor is efficient and stable, being able of responding to disturbances in methane feed concentration. It is advisable to design the reactor for the average methane concentration, and then test by means of simulations the capability of this design to maintain stable operation for typical concentration disturbances present in the emission.

When the magnitude of disturbances can produce reactor extinction or overheating, the use of a control system is recommended. In this case, the reactor can be designed to maintain stable operation for the lowest methane feed concentration. Then, the control system is designed to deal with high methane concentration disturbances, avoiding overheating. Many different control strategies have been proposed and tested for reverse flow reactors [31].

3.5. Economic optimisation of the reverse flow reactor with integrated adsorption

The cost is a very important factor to consider when a new reactor is going to be implemented. Given that, this reverse flow reactor with integrated adsorption is a new and innovative approach in this subject, the total cost will be optimised for the actual case from section 3.2, considering the operational conditions: switching time and gas velocity.

The methodology to optimise the cost is described afterwards. Firstly, a switching time and a gas velocity are chosen and the MATLAB code is used to calculate the length of the reactor and the catalytic fraction, as explained in section 3.2. Then, the cost of the reactor and also a fan required for the gas flow are calculated [32]. The fan power was calculated from an energy balance (Bernouilli equation) and considering a fan efficiency of 85%. The reactor cost was estimated considering it as a stainless steel framework. The prices for the catalyst, adsorbent and inert were provided by BASF. The Lang factorial method [32] was used to estimate the fixed capital cost of a project from the costs of the major equipment units. One of these factors estimates the cost of instrumentation, pipes and connections, while other considers the indirect costs such as contingencies, set-up and maintenance. The variable costs consist basically of the electricity consumed by the fan and the replacement of the catalyst, inert and adsorbent every five years. Deducting start-up and maintenance times, a basis of 320 days per

year can be used as a representative rate for a large company. The variable costs were calculate over a timeframe of 10 years.

The parametric analysis for the cost was carried out as follows: 170 $\leq t_{sw} \leq$, 390 s and 0.75 $\leq v \leq$ 1.4 m/s. From the practical point of view, the minimum values for the switching time and gas velocity are set to 170 s and 0.75 m/s, respectively. Figure 10 shows a contour chart where total cost in M€ has been plotted as a function of the switching time and the gas velocity. An optimal can be found for a switching time of 250 s and a gas velocity of 1.13 m/s.

The topology of the optimum should be taken into account to select the optimum operating conditions. Thus, the gas velocity should be fixed at v = 1.13 m/s, because an optimum at this value is clearly observed. As the gas velocity decreases, the total cost exhibits an increase of 50%; the same increase in the cost is observed on increasing the gas velocity to 1.26 m/s. On the contrary, the switching time produces a wider optimum at t_{sw} = 240-260 s, which means that within this range costs do not change dramatically. A recommend switching time value of 240 s was found in literature [29], which is in agreement with the findings of the present economic optimization.

Considering an optimal case of v = 1.13 m/s and t_{sw} = 250 s, the reactor length would be 1.43 m with a catalytic fraction of 29%. The total cost for this case would be 1.57 M€. However, if this case is re-designed without using integrated adsorption, the total cost would increase to 1.77 M€. The main individual and total costs are summarized in Figure 11. When no adsorbent is used, reaction rate decreases and more catalyst is required to maintain the same conversion. Hence, the catalyst amount increases, but also the reactor framework size, as observed in Figure 11. This affects both fixed capital and 10-year variable costs. The later takes into account the replacement of the catalyst, which is an important contribution. These two costs, reactor framework and catalyst, are the two main costs of the reverse flow reactor project, and for this reason the use of adsorbent contributes to reduce the total cost in 14%.

4. Conclusions

The use regenerative catalytic oxidation in a novel reverse flow reactor with integrated adsorption is proposed to treat coal mine ventilation air methane emissions. The novelty of this reactor is the use of an adsorbent material to separate water from the ventilation air, where the concentration is as high as 2-5% (mol), and avoid the inhibition of the catalyst.

The reverse flow reactor has been designed for 45 m^3/s (1 atm, 25°C) of ventilation air with 0.30% (mol) of methane and 5% of water. The computer simulations have shown that the adsorbent is capable of self-regenerate in situ by means of the switch of the flow direction and the parabolic temperature profile. Thus, when one of the adsorbent beds is adsorbing the feed water, the other is being regenerated by the displacement of the high temperature of the middle of the reactor. This design has been tested against typical variations in the concentration of methane in the ventilation air of a real coal mine. The simulations shown that the reactor is affected, but does not extinguish.

The operating conditions of the reactor with integrated adsorption have been optimized by the minimization of the total cost (fixed capital and 10-year variable). A gas velocity of 1.13 m/s and a switching time of 240-260 s were found to be optimum.

Acknowledgements

This work was supported by the Research Fund for Coal and Steel of the European Union (contract UE-10-RFCS-CT-2010-00004), and by the Local Asturian Government (FC-15-GRUPIN14-078)

Nomenclature

a	surface to bed volume ratio (m^2/m^3_{bed})
c_i	gas molar concentration (mol/m^3)
C_P	heat capacity (J/kg k)
D_{im}	molecular diffusion coefficient (m^2/s)
D_{ax}	axial dispersion coefficient (m^2/s)
D_{ep}	effective pore diffusion coefficient (m^2/s)
D_h	hydraulic diameter of the monolith (m)
d_P	particle diameter (m)
f_w	washcoating fraction (%)
h	gas to solid heat transfer coefficient (W/m^2 K)
k	thermal conductivity (W/m K)
K_{eqi}	water adsorption equilibrium constant (mol/kg_{ads})$(m^3/mol)^{0.5}$
K_{inh}	water inhibition constant (1/Pa)
L_w	washcoating size (m)
K_C	gas-solid mass transfer coefficient (m/s)
k_w	kinetic constant (mol/kg_{cat} s Pa)
L_R	reactor length (m)
m	Freundlich exponent
n_i	concentration in the solid (mol/kg)
Nu	Nusselt number ($\mathrm{Nu} = hD_h/k_G$)
p	Pressure (Pa)
Pr	Prandtl number ($\mathrm{Pr} = C_{PG}\mu_G/k_G$)
Re	Reynolds number ($\mathrm{Re} = D_h v\rho_G/\mu_G$)

r_i	reaction rate (mol/kg s)
R	ideal gas constant (8.314 J/mol K)
Sc	Schmidt number ($\mathrm{Sc} = \mu_G/(\rho_G D_{im})$)
Sh	Sherwood number ($\mathrm{Sh} = K_C D_h/D_{im}$)
t	time (s)
T	temperature (K)
T_{ph}	pre-heating temperature (K)
t_{sw}	switching time (s)
v	gas (interstitial) velocity (m/s)
y	mole fraction (-)
z	spatial coordinate (m)

Greek symbols

ϵ_b	bed porosity (-)
ΔH_i	reaction enthalpy (-802.5 kJ/mol)
ϕ	Thiele modulus (-)
κ_{Gax}	axial dispersion coefficient for the gas phase (W/m K)
η	internal effectiveness factor (-)
ρ	density (kg/m^3)

Subscripts

0	inlet
cat	catalyst
G	gas
S	solid

Caption to figures

Figure 1 Sketch of the reverse flow reactor with integrated adsorption.

Figure 2 Monitoring of methane concentration in the ventilation air of mine site 1.

Figure 3 Evolution of temperature (a) and methane concentration (b) profiles during a cycle at the pseudo-steady state: begin (—), middle (—) and end (—) of cycle. The arrow indicates the direction of the flow.

Figure 4 Evolution of water gas concentration (a) and water solid concentration (b) profiles during a cycle at the pseudo-steady state: begin (—), middle (—) and end (—) of cycle. Water feed mole fraction = 0.05. The arrow indicates the direction of the flow.

Figure 5 Evolution of water mole fraction in the effluent of the reactor.

Figure 6 Water gas concentration (a) and water solid concentration (b) profiles in the inert beds (BED1 and BED2) at the end of a cycle (the arrow indicates the direction of the flow). Feed water mole fraction: 0.02 (—), 0.03 (—), 0.04 (—) and 0.05 (—).

Figure 7 Capacity of the reverse flow reactor design to deal with disturbances in methane feed concentration. Temperature (a) and methane concentration (b) profiles (middle of cycle): pseudo-steady state at 0.30% methane (•••), after 16 min (4 cycles) at 0.27% methane (—), and after other 16 min (4 cycles) another time at 0.30% methane (—).

Figure 8 Performance of the reverse flow reactor with integrated adsorption for methane changes in a real ventilation air emission: evolution of inlet (—) and outlet (—) methane concentration. Switching time = 240 s.

Figure 9 Performance of the reverse flow reactor with integrated adsorption for methane changes in a real ventilation air emission: evolution of temperature (a) and

methane concentration (b) profiles (profiles corresponding to the middle of a cycle). Switching time = 240 s. Lines correspond to times (in min): 120 (▬), 144 (▬), 168 (▬), 192 (•••) and 216 (•••).

Figure 10 Optimisation of the total cost (M€) as a function of the switching time and the gas velocity for a reverse flow reactor with integrated adsorption.

Figure 11 Contribution of main individual costs and total costs (fixed capital and 10-yr variable) for reverse flow reactor with (■) and without (■) integrated adsorption.

Figure 1

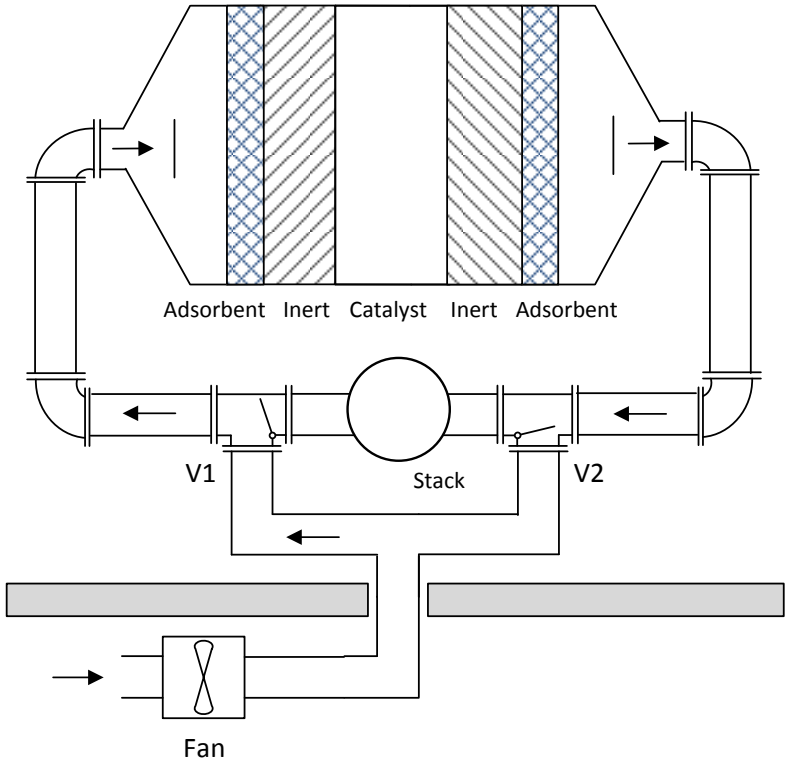

Figure 2

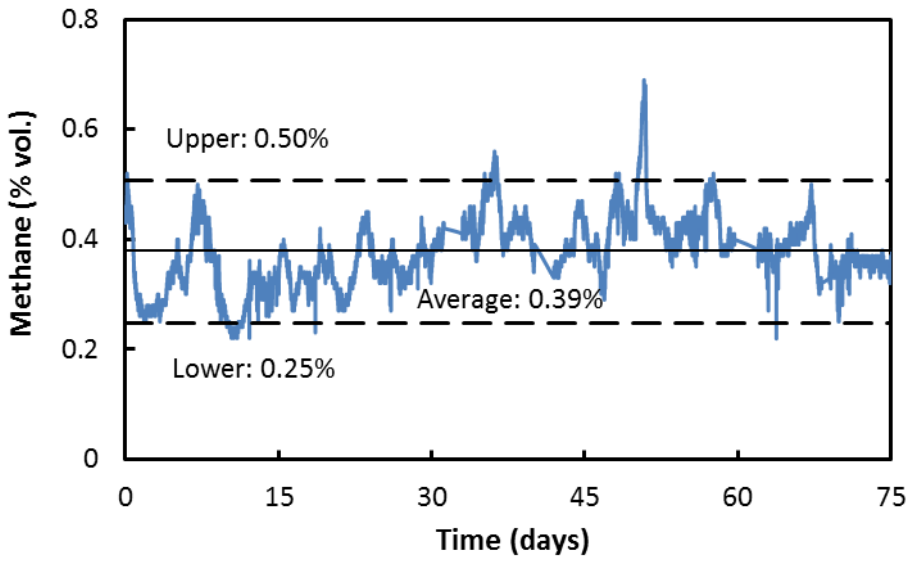
0.8
0.6
0.4
0.2
0
Methane (% vol.)
Upper: 0.50%
Average: 0.39%
Lower: 0.25%
0
15
30
45
60
75
Time (days)

Figure 3

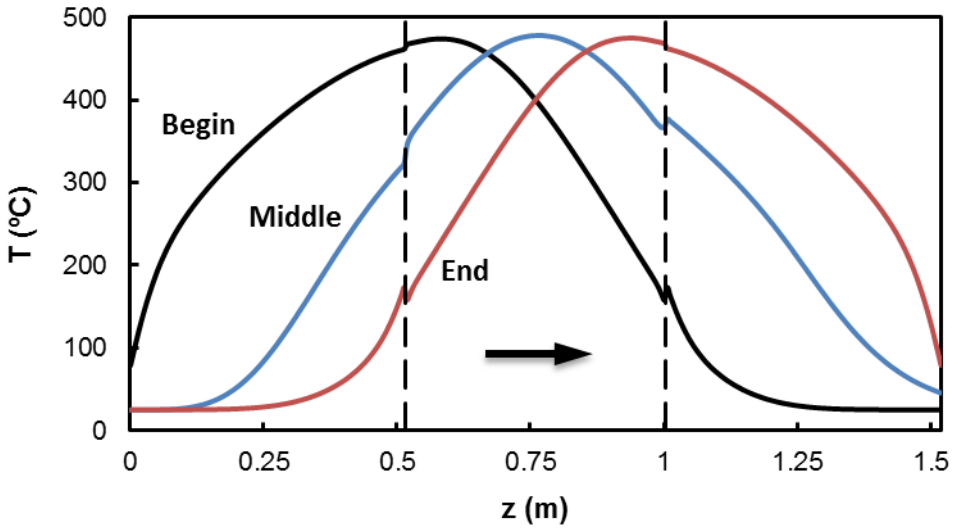
500
400
300
200
100
0
T (°C)
Begin
Middle
End
0
0.25
0.5
0.75
1
1.25
1.5
z (m)

(a)

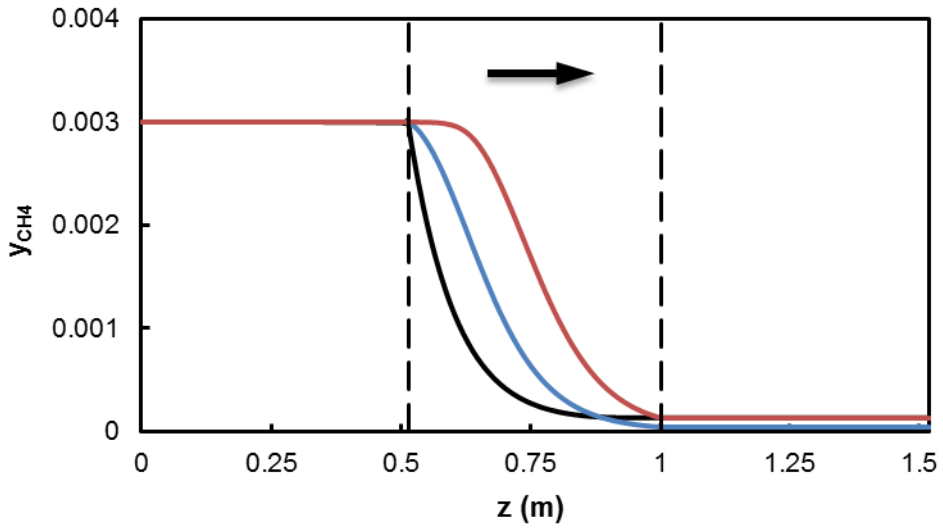
0.004
0.003
0.002
0.001
0
y_{CH4}
0
0.25
0.5
0.75
1
1.25
1.5
z (m)

(b)

Figure 4

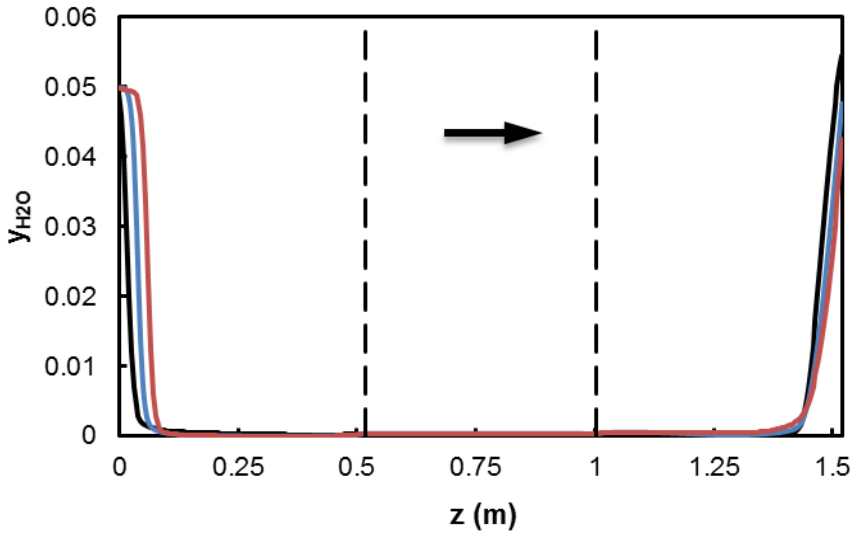
0.06
0.05
0.04
0.03
0.02
0.01
0
y_{H2O}
0
0.25
0.5
0.75
1
1.25
1.5
z (m)

(a)

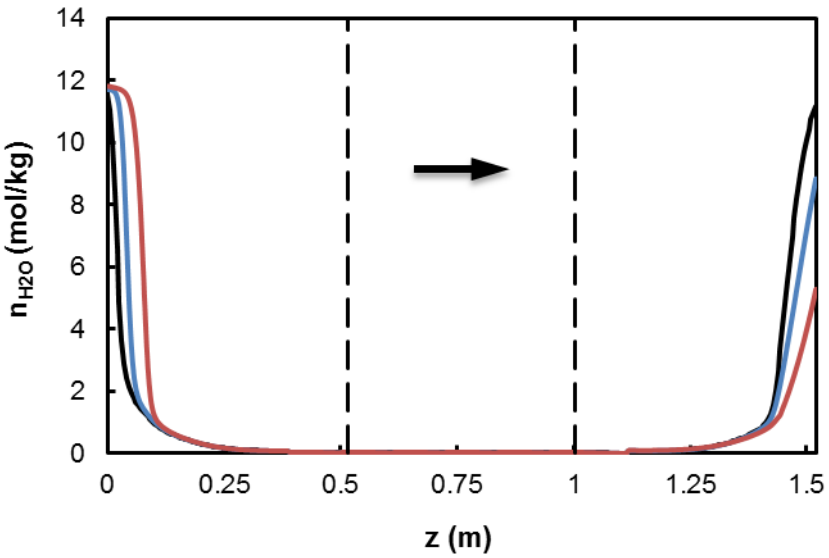
14
12
10
8
6
4
2
0
n_{H2O} (mol/kg)
0
0.25
0.5
0.75
1
1.25
1.5
z (m)

(b)

Figure 5

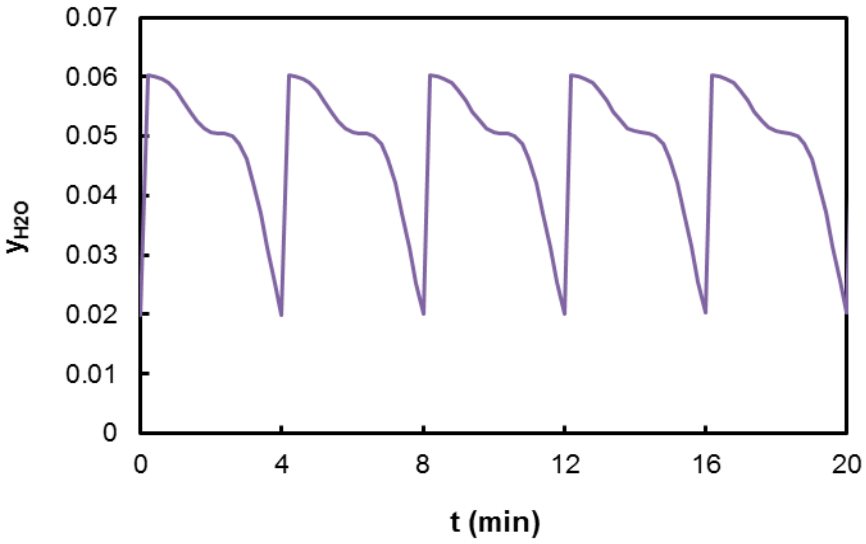

Figure 6

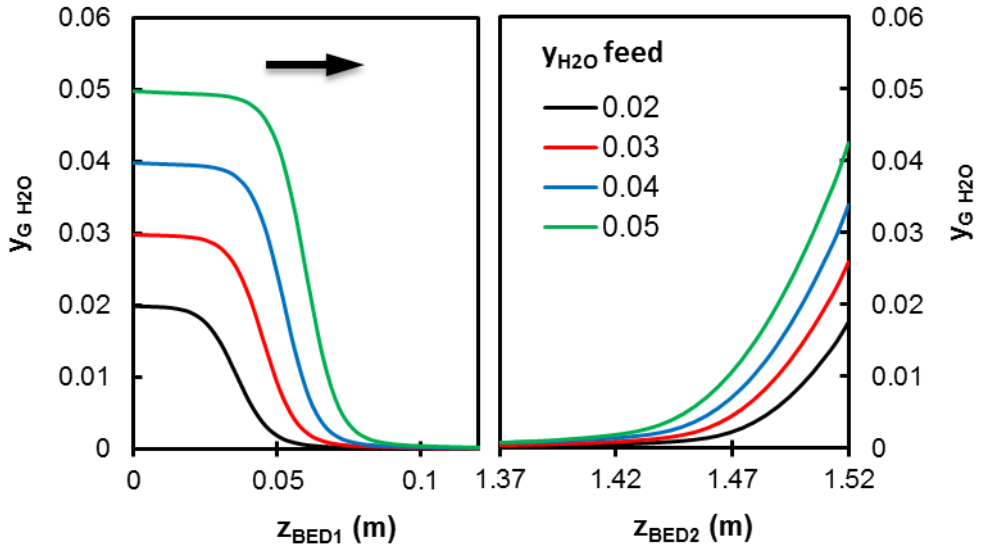
0.06
0.05
0.04
0.03
0.02
0.01
0
$y_{G\ H2O}$
0
0.05
0.1
1.37
1.42
1.47
1.52
z_{BED1} (m)
z_{BED2} (m)
y_{H2O} feed
0.02
0.03
0.04
0.05

(a)

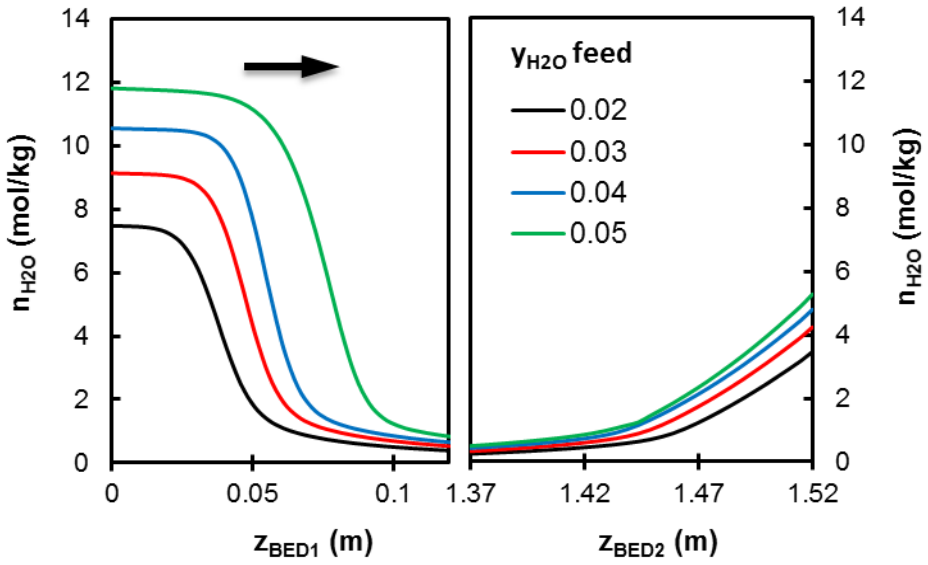
14
12
10
8
6
4
2
0
n_{H2O} (mol/kg)
0
0.05
0.1
1.37
1.42
1.47
1.52
z_{BED1} (m)
z_{BED2} (m)
y_{H2O} feed
0.02
0.03
0.04
0.05

(b)

Figure 7

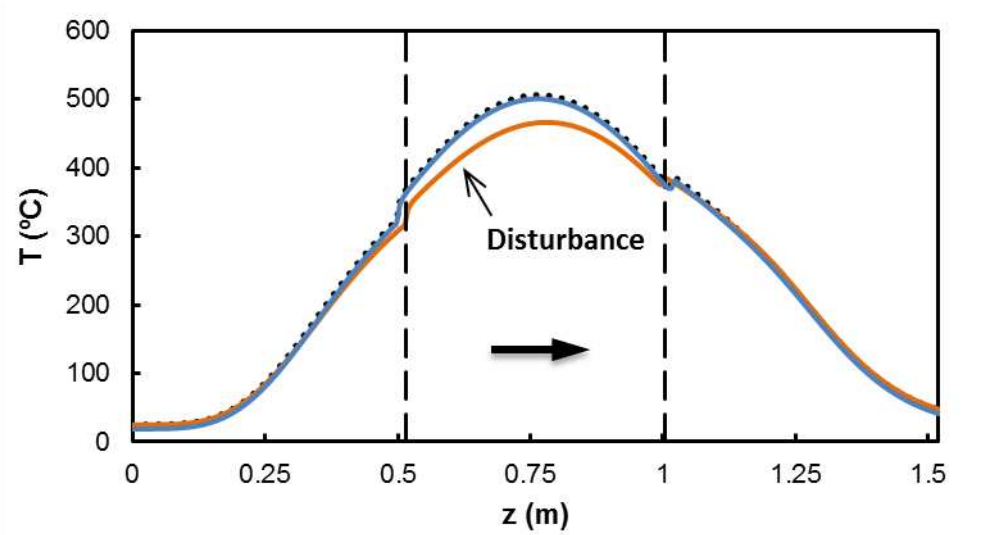
600
500
400
300
200
100
0
T (°C)
Disturbance
0
0.25
0.5
0.75
1
1.25
1.5
z (m)

(a)

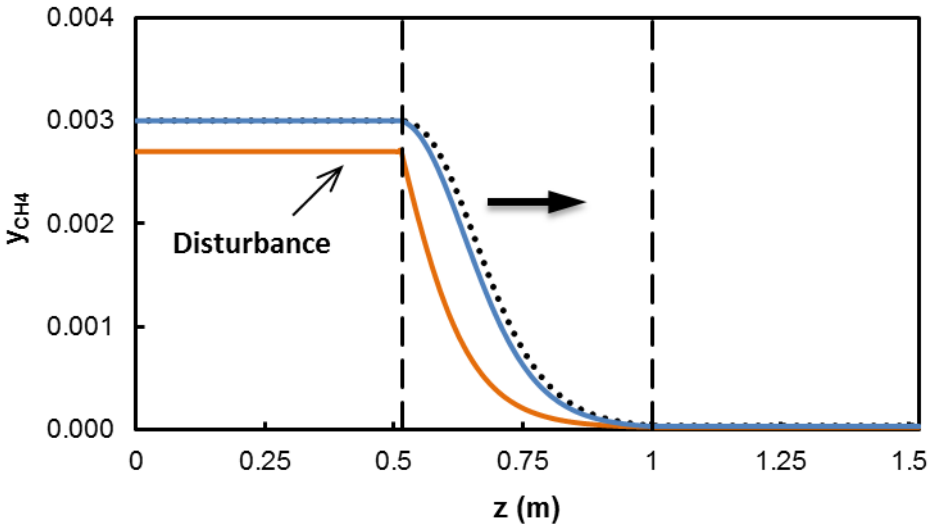
0.004
0.003
0.002
0.001
0.000
y_{CH4}
Disturbance
0
0.25
0.5
0.75
1
1.25
1.5
z (m)

(b)

Figure 8

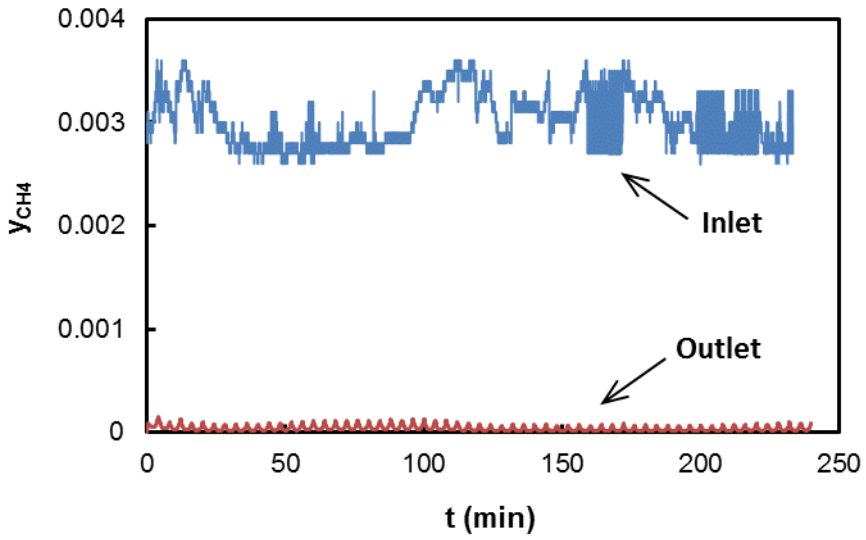
0.004
0.003
0.002
0.001
0
y_{CH4}
Inlet
Outlet
0
50
100
150
200
250
t (min)

Figure 9

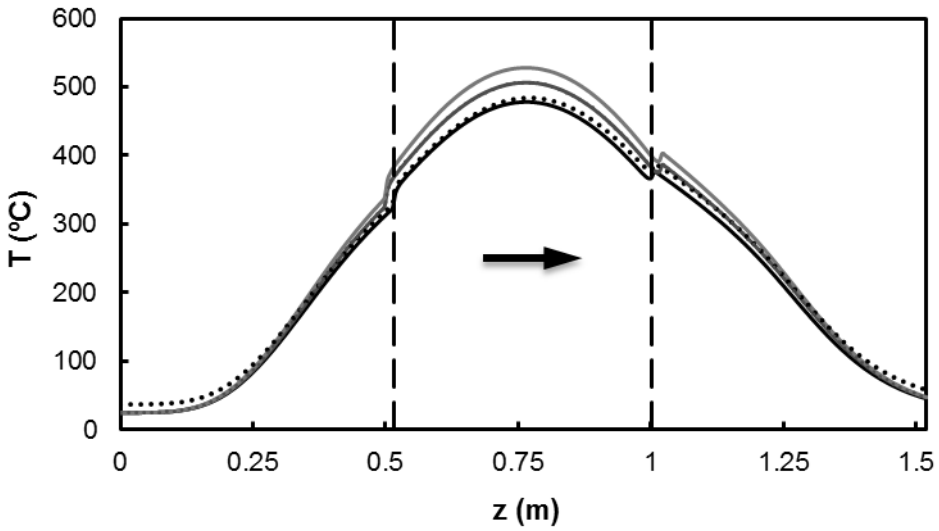
600
500
400
300
200
100
0
T (°C)
0
0.25
0.5
0.75
1
1.25
1.5
z (m)

(a)

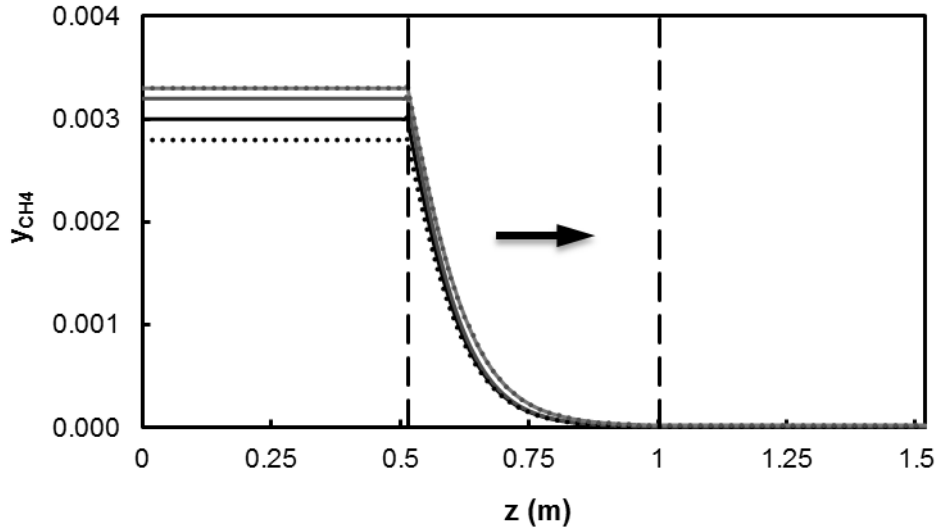
0.004
0.003
0.002
0.001
0.000
yCH4
0
0.25
0.5
0.75
1
1.25
1.5
z (m)

(b)

Figure 10

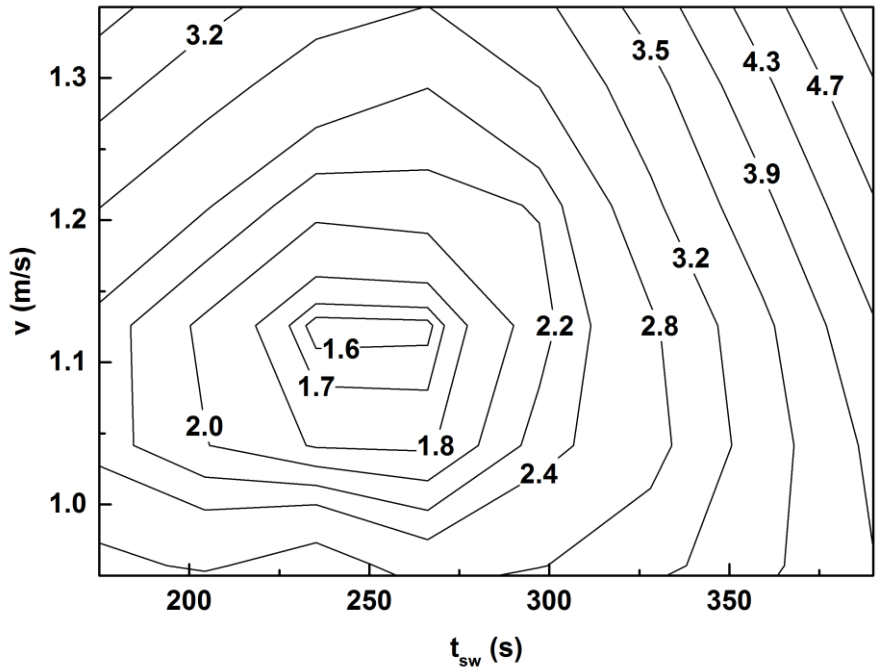
3.2
3.5
4.3
4.7
3.9
3.2
2.8
2.2
1.6
1.7
2.0
1.8
2.4
1.3
1.2
1.1
1.0
v (m/s)
200
250
300
350
t_sw (s)

1 Figure 11

2

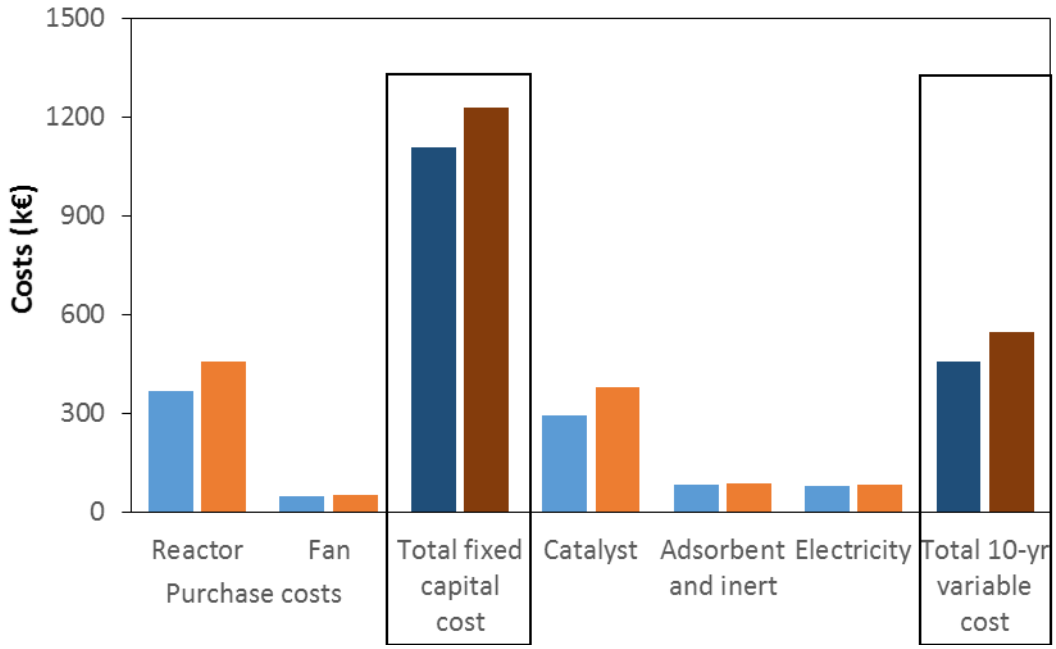

3

Tables

Table 1 Conservation equations for the reverse flow reactor with integrated adsorption: heterogeneous 1D dynamic model.

Mass balances
$$\frac{\partial c_i}{\partial t} = -v\frac{\partial c_i}{\partial z} + D_{ax}\frac{\partial^2 c_i}{\partial z^2} - \frac{aK_C}{\epsilon_b}(c_i - c_{Si})$$
$$\frac{\partial n_i}{\partial t} = \frac{aK_C}{\rho_S(1-\epsilon_b)}(c_i - c_{Si}) + \eta r_i$$
Energy balances
$$\frac{\partial T_G}{\partial t} = -v\frac{\partial T_G}{\partial z} + \frac{\kappa_{Gax}}{\rho_G C_{PG}}\frac{\partial^2 T_G}{\partial z^2} + \frac{ah}{\rho_G C_{PG}\epsilon_b}(T_S - T_G)$$
$$\frac{\partial T_S}{\partial t} = \frac{k_S}{\rho_S C_{PS}}\frac{\partial^2 T_S}{\partial z^2} + \frac{ah}{\rho_S C_{PS}(1-\epsilon_b)}(T_G - T_S) + \frac{\rho_{cat}\eta r_i \Delta H_i}{\rho_S C_{PS}}$$

i = CH_4, H_2O

Table 2 Initial and boundary conditions for the reverse flow reactor with integrated adsorption.

Initial conditions	
$c_i\|_{t=0} = n_i\|_{t=0} = 0$	$T_G\|_{t=0} = T_S\|_{t=0} = T_{ph}$
Boundary conditions	
$(c_i)_{0^-} = (c_i)_{0^+} - \frac{D_{ax}}{v}\left(\frac{\partial c_i}{\partial z}\right)_{0^+}$	$(T_G)_{0^-} = (T_G)_{0^+} - \frac{\kappa_{Gax}}{v\rho_G C_{PG}}\left(\frac{\partial T_G}{\partial z}\right)_{0^+}$
$\left(\frac{\partial c_i}{\partial z}\right)_{z=L_R} = 0$	$\left(\frac{\partial T_S}{\partial z}\right)_{z=0^+} = 0$
	$\left(\frac{\partial T_G}{\partial z}\right)_{z=L_R} = \left(\frac{\partial T_S}{\partial z}\right)_{z=L_R} = 0$

Table 3 Geometric and physical properties of the catalytic and adsorbent beds [22].

Bed properties	**Catalytic bed**	**Adsorbent bed**
Characteristic length, D_h / d_P	10^{-3} m	4×10^{-3} m
Bed porosity, ϵ_b	63%	40%
Solid density, ρ_S	2300 kg/m^3	1060 kg/m^3
Solid heat capacity, C_{PS}	900 J/kg K	836 J/kg K
Solid thermal conductivity, k_S	2 W/m K	0.5 W/m K
Thermal inertia, $\rho_S(1-\epsilon_b)C_{PS}$	766 kJ/m$^3_{\text{bed}}$ K	532 kJ/m$^3_{\text{bed}}$ K

Table 4 Expressions used to calculate physical, chemical and transport properties.

Catalytic bed	
Kinetic equation (methane) [25]	$r_{CH_4} = -\dfrac{k_w p_{CH_4}}{1 + K_{inh} p_{H_2O}} = -k'_w p_{CH_4}$ $k_w = 1.56\, e^{-80000/RT_S}$ mol/(kg$_{monolith}$ s Pa) $K_{inh} = 8.07 \times 10^{-9}\, e^{67600/RT_S}$ Pa^{-1}
Effectiveness factor (methane) [25]	$\eta = \dfrac{\tanh \phi}{\phi}, \qquad \phi = L_w \sqrt{\dfrac{k'_w \rho_{cat} R T_S}{f_w\, D_{ep}}}$
Surface to volume ratio of the bed	$a = (4/D_h)\, \epsilon_b$
Mass transfer (methane) [25]	$K_C = (D_{im}/D_h)$ Sh, Sh = 2.977 (laminar)
Heat transfer [25]	$h = (k_g/D_h)$ Nu, Nu = 2.977 (laminar)
Axial dispersion (mass) [26]	$D_{ax} = D_h v \left[\dfrac{1}{\mathrm{Re\,Sc}} + \dfrac{\mathrm{Re\,Sc}}{192}\right]$
Axial dispersion (energy) [26]	$\kappa_{Gax} = D_h v \rho_G C_{PG} \left[\dfrac{1}{\mathrm{Re\,Pr}} + \dfrac{\mathrm{Re\,Pr}}{192}\right]$
Adsorbent bed	
Adsorption equilibrium (water) [22]	$n_i^* = K_{eqi} {c_i}^m \;\rightarrow\; c_{Si} = \left(n_i/K_{eqi}\right)^{1/m}$, m = 0.5 $K_{eqi} = 1.14\, e^{4700/RT_S}$ (mol/kg$_{ads}$)(m^3/mol)$^{0.5}$
Surface to volume ratio of the bed	$a = (6/d_P)(1 - \epsilon_b)$
Global mass transfer (water) [22]	$K_C = 0.22\, (T_S/373)^{-3.6}$ m/s
Heat transfer [26]	$h = \left(k_g/d_P\right)$ Nu, $\mathrm{Nu} = 2 + Re^{1/2} Pr^{1/3}$
Axial dispersion (mass) [26]	$D_{ax} = d_P v \left[\dfrac{0.73}{\mathrm{Re\,Sc}} + \dfrac{0.5}{1 + \dfrac{9.7}{\mathrm{Re\,Sc}}}\right]$
Axial dispersion (energy) [26]	$\kappa_{G,ax} = d_P v \rho_G C_{PG} \left[\dfrac{0.73}{\mathrm{Re\,Pr}} + \dfrac{0.5}{1 + \dfrac{9.7}{\mathrm{Re\,Pr}}}\right]$

R = 8.314 J/mol K

Table 5 Composition of the ventilation air from different coal mine sites (concentrations in % Vol.)

Coal mine	Coal production (kt/year)	Average methane concentration	Water concentration
Site 1	187	0.40	2.0-4.0
Site 2	141	0.40	2.3-2.9
Site 3	334	0.20	3.3-4.0
Site 4	106	0.18	2.6-5.0

References

[1] NOAA, http://www.esrl.noaa.gov/gmd/ccgg/figures/, in.

[2] I. Karakurt, G. Aydin, K. Aydiner, Mine ventilation air methane as a sustainable energy source, Renewable and Sustainable Energy Reviews, 15 (2011) 1042-1049.

[3] S. Su, A. Beath, H. Guo, C. Mallett, An assessment of mine methane mitigation and utilisation technologies, Progress in Energy and Combustion Science, 31 (2005) 123-170.

[4] K. Shah, B. Moghtaderi, E. Doroodchi, J. Sandford, A feasibility study on a novel stone dust looping process for abatement of ventilation air methane, Fuel Processing Technology, 140 (2015) 285-296.

[5] E. Díaz, J. Fernández, S. Ordóñez, N. Canto, A. González, Carbon and ecological footprints as tools for evaluating the environmental impact of coal mine ventilation air, Ecological Indicators, 18 (2012) 126-130.

[6] K. Gosiewski, A. Pawlaczyk, Catalytic or thermal reversed flow combustion of coal mine ventilation air methane: What is better choice and when?, Chemical Engineering Journal, 238 (2014) 78-85.

[7] Z. Yang, P. Yang, L. Zhang, M. Guo, J. Ran, Experiment and modeling of low-concentration methane catalytic combustion in a fluidized bed reactor, Applied Thermal Engineering, 93 (2016) 660-667.

[8] S. Su, J. Agnew, Catalytic combustion of coal mine ventilation air methane, Fuel, 85 (2006) 1201-1210.

[9] P. Marín, S. Ordóñez, F.V. Díez, Procedures for heat recovery in the catalytic combustion of lean methane-air mixtures in a reverse flow reactor, Chemical Engineering Journal, 147 (2009) 356-365.

[10] D. Fissore, A.A. Barresi, G. Baldi, M.A-G. Hevia, S. Ordóñez, F.V. Díez, Design and testing of small-scale unsteady state afterburners and reactors, AIChE Journal, 51 (2005) 1654-1664.

[11] K. Gosiewski, A. Pawlaczyk, M. Jaschik, Energy recovery from ventilation air methane via reverse-flow reactors, Energy, 92 (2015) 13-23.

[12] G. Eigenberger, G. Kolios, U. Nieken, Thermal pattern formation and process intensification in chemical reaction engineering, Chemical Engineering Science, 62 (2007) 4825-4841.

[13] S. Wang, D. Gao, S. Wang, Steady and transient characteristics of catalytic flow reverse reactor integrated with central heat exchanger, Industrial and Engineering Chemistry Research, 53 (2014) 12644-12654.

[14] X. Zheng, Y. Shi, X. Wang, N. Cai, Elementary reaction modeling of methane catalytic combustor: Effects of hysteresis in pd-based catalyst activity, Combustion Science and Technology, 187 (2014) 1044-1064.

[15] Z. Li, Z. Qin, Y. Zhang, Z. Wu, H. Wang, S. Li, R. Shi, M. Dong, W. Fan, J. Wang, A control strategy of flow reversal with hot gas withdrawal for heat recovery and its application in mitigation and utilization of ventilation air methane in a reverse flow reactor, Chemical Engineering Journal, 228 (2013) 243-255.

[16] P. Hurtado, S. Ordóñez, H. Sastre, Dı, amp, x, F.V. ez, Combustion of methane over palladium catalyst in the presence of inorganic compounds: inhibition and deactivation phenomena, Applied Catalysis B: Environmental, 47 (2004) 85-93.

[17] K. Persson, L.D. Pfefferle, W. Schwartz, A. Ersson, S.G. Järås, Stability of palladium-based catalysts during catalytic combustion of methane: The influence of water, Applied Catalysis B: Environmental, 74 (2007) 242-250.

[18] J.-H. Park, J.H. Cho, Y.J. Kim, E.S. Kim, H.S. Han, C.-H. Shin, Hydrothermal stability of Pd/ZrO2 catalysts for high temperature methane combustion, Applied Catalysis B: Environmental, 160–161 (2014) 135-143.

[19] A.N.R. Bos, J.P. Lange, G. Kabra, A novel reverse flow reactor with integrated separation, Chemical Engineering Science, 62 (2007) 5661-5662.

[20] C. Urbani, P. Marín, F.V. Díez, S. Ordóñez, Catalytic combustion of sulphur-containing methane lean emissions in a reverse-flow reactor with integrated adsorption, Chemical Engineering Journal, 285 (2016) 39-48.

[21] J. Kallrath, A. Schreieck, B. Brockmüller, D.W. Agar, O. Watzenberger, S.A.E.G. Falle, J.R. Giddings, Simulation of chromatographic reactors, Computers & Chemical Engineering, 18 (1994) S331-S335.

[22] J. Fernández, P. Marín, F.V. Díez, S. Ordóñez, Experimental demonstration and modeling of an adsorption-enhanced reverse flow reactor for the catalytic combustion of coal mine ventilation air methane, Chemical Engineering Journal, 279 (2015) 198-206.

[23] G. Groppi, E. Tronconi, P. Forzatti, Mathematical Models of Catalytic Combustors, Catalysis Reviews, 41 (1999) 227 - 254.

[24] P. Marín, S. Ordóñez, F.V. Díez, Monoliths as suitable catalysts for reverse-flow combustors: modelign and experimental validation, AIChE Journal, 56 (2010) 3162-3173.

[25] J. Fernández, P. Marín, F.V. Díez, S. Ordóñez, Coal mine ventilation air methane combustion in a catalytic reverse flow reactor: Influence of emission humidity, Fuel Processing Technology, 133 (2015) 202-209.

[26] C.R. Thompson, P. Marín, F.V. Díez, S. Ordóñez, Evaluation of the use of ceramic foams as catalyst supports for reverse-flow combustors, Chemical Engineering Journal, 221 (2013) 44-54.

[27] D.W. Green, R.H. Perry, Perry's Chemical Engineers' Handbook, 8th ed., McGraw-Hill, 2008.

[28] P. Marín, M.A.G. Hevia, S. Ordóñez, F.V. Díez, Combustion of methane lean mixtures in reverse flow reactors: Comparison between packed and structured catalyst beds, Catalysis Today, 105 (2005) 701-708.

[29] A.A. Barresi, G. Baldi, D. Fissore, Forced unsteady-state reactors as efficient devices for integrated processes: Case histories and new perspectives, Industrial & Engineering Chemistry Research, 46 (2007) 8693-8700.

[30] P. Marín, S. Ordóñez, F.V. Díez, Simplified design methods of reverse flow catalytic combustors for the treatment of lean hydrocarbon–air mixtures, Chemical Engineering and Processing: Process Intensification, 48 (2009) 229-238.

[31] P. Dufour, Y. Toure, Multivariable model predictive control of a catalytic reverse flow reactor, Computers & Chemical Engineering, 28 (2004) 2259-2270.

[32] M. Peters, K. Timmerhaus, R. West, Plant Design and Economics for Chemical Engineers, McGraw-Hill Education, 2003.